scientific reports

Check for updates

OPEN

GliaTrap is a biodegradable, non-swelling and non-inflammatory hydrogel with tuned release of CXCL12 to attract migrating glioblastoma cells

Yusuke Suita[1], Saradha Miriyala[1], Deniz Merih-Toruner[1], Mattia Pizzagalli[1], Owen P. Leary[1], Weizhou Yue[2], Lingxiao Xie[2], Blessing Akobundu[1], Nathan Pertsch[3], Andras Fiser[5], Eduardo Fajardo[5], Jie Shen[6] & Nikos Tapinos[1,4]✉

A significant factor in relapse and dismal prognosis of glioblastoma is the migrating glioblastoma cells, which diffuse away from the tumor mass into the brain parenchyma. Post-resection application of biomaterials to deliver cytotoxic agents against the invading glioblastoma cells has recently gained attention. The aim of this study was to develop a non-swelling, non-inflammatory biomimetic hydrogel with sustained release of a chemoattractant for glioblastoma cells and perform in vivo proof-of-concept studies to show chemoattraction of invading glioblastoma cells in orthotopic models of human glioblastoma. We used hyaluronic/collagen II-based (HA/Col) hydrogel that incorporates liposomes loaded with CXCL12 to develop GliaTrap. Sustained release of CXCL12 was measured with an ELISA assay. The non-inflammatory properties of GliaTrap were assessed in-vivo after stereotactic implantation in the mouse brain using a cytokine array and immunohistochemistry. The efficacy of GliaTrap on attracting GSCs was determined in-vivo employing 3D light-sheet microscopy on orthotopic human glioblastoma xenografts. We show that GliaTrap is an injectable, non-swelling biomimetic hydrogel that attains sustained release of CXCL12 and does not induce inflammation in the mouse brain. GliaTrap significantly attracts invading glioblastoma cells in orthotopic xenograft models of human glioblastoma as shown with 3D light sheet microscopy. Our findings indicate that GliaTrap can be safely used to attract invading glioblastoma cells by sustained release of a chemoattractant without inducing inflammatory conditions in the brain or local swelling.

Glioblastoma is the most malignant and aggressive primary brain tumor with an average overall survival of 16 ~ 21 months after initial diagnosis[1]. Standard treatment of glioblastoma includes surgical resection followed by radiation in the vicinity of the resection cavity and administration of temozolomide[2]. Even with this therapeutic approach, tumor recurrence is inevitable[3] primarily due to the presence of glioma stem cells (GSCs), which are characterized by high migratory potential[4–6], resistance to chemotherapy and radiation, and the ability to form recurrent tumors[7]. Eradication of the invading GSCs remains an unmet medical need that contributes to the high recurrence rate of glioblastoma.

To start addressing this challenge, we engineered GliaTrap to sequester the majority of the invading glioblastoma cells in the proximity of the tumor resection cavity. GliaTrap is a biodegradable non-swelling hydrogel which could be implanted into the tumor resection cavity after surgery. A chemoattractant concentration gradient is maintained by the hydrogel to lure residual glioblastoma cells to the vicinity of the hydrogel. By design, GliaTrap is comprised primarily of biopolymers that are abundant in the human body: collagen and hyaluronic acid (HA). It has been shown that collagen-based in situ hydrogels can quickly form a gel at 37 °C[8,9] and most of the collagen

[1]Laboratory of Cancer Epigenetics and Plasticity, Brown University, Rhode Island Hospital, 593 Eddy Street, Providence, RI 02903, USA. [2]Departments of Biomedical and Pharmaceutical Sciences and Chemical Engineering, University of Rhode Island, Kingston, RI, USA. [3]Rush University Medical Center, Chicago, IL, USA. [4]Department of Neurosurgery, Warren Alpert Medical School, Brown University, Providence, RI, USA. [5]Department of Systems and Computational Biology, Albert Einstein College of Medicine, Bronx, NY, USA. [6]Department of Pharmaceutical Sciences, Northeastern University, Boston, MA, USA. ✉email: nikos_tapinos@brown.edu

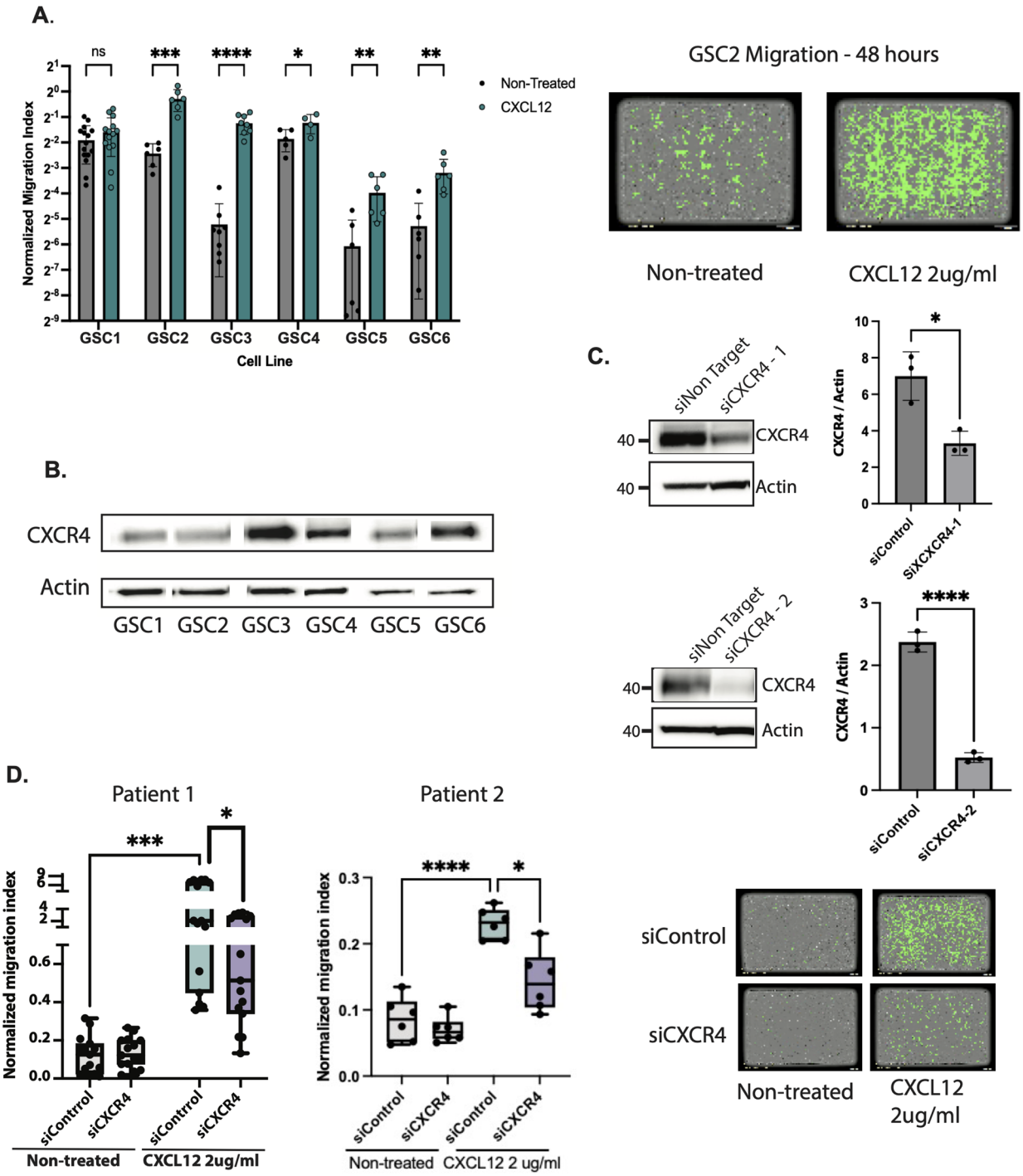

isoforms have been shown to have functional contributions to various functions of the developing and adult brain[10]. GliaTrap is composed of a mixture of HA/collagen II (Col II) since this combination showed excellent non-swelling characteristics, prolonged release of the chemoattractant and good biocompatibility profile for brain tissue as it has been shown before for other HA/Col II hydrogels[11].

The C-X-C motif chemokine ligand-12/C-X-C motif chemokine receptor-4 (CXCL12/CXCR4) signaling axis is involved in central nervous system (CNS) development[12], while in glioblastoma, it has been shown that it is important for invasion[13], GSC migration and therapeutic resistance[14]. Due to its known role in promoting migration, we decided to use CXCL12 as a chemoattractant for our GliaTrap proof-of-principle study. We developed our HA/Col II-based hydrogel for the release of CXCL12 and characterized it to be both non-swelling and injectable. To achieve sustained release of CXCL12 in the brain, we encapsulated CXCL12 within nano-liposomes and showed continuous CXCL12 release in an artificial cerebrospinal fluid (CSF) over several weeks. We showed that either GliaTrap (CXCL12 + hydrogel) or the hydrogel alone do not induce significant inflammatory effects in the brain in vivo, hence they could be safely applied in a clinical oncology setting. Using

◀**Fig. 1**. CXCL12 induces GSC chemotaxis via CXCR4 receptor. (**A**) Chemotaxis assay of 6 patients derived GSCs treated with 2 ug/ml CXCL12. Images were taken at 48 h using Incucyte Live cell imaging (Sartorius). Left panel shows normalized migration index ([GSC's area in bottom well]/GSC's area in top well)) at 48 h compared to non-treated GSCs. CXCL12 induces significant increase in GSC migration ($n = 6$–14 per GSC, $^{*}p < 0.05$, $^{**}p < 0.001$, $^{***}p < 0.00005$, $^{****}p < 0.000001$, Student's t-test). Right panel shows representative images of migrating GSCs (objects with the green "mask") in bottom well at 48 h (left: non-treated, right: 2 ug/ml CXCL12). (**B**) Expression of CXCR4 in 6 patients derived GSCs. (**C**) Representative Western blot showing inhibition of CXCR4 expression with two independent siRNAs. Quantification of CXCR4 after siRNA inhibition shows that both siRNAs significantly inhibit CXCR4 expression but siCXCR4-2 showed a better response ($n = 3$, $^{*}p < 0.05$, $^{***}p < 0.0001$, Student's t-test). Actin was used as loading control. (**D**) Chemotaxis assay of 2 patient-derived GSCs treated with 50 nM siCXCR4 for 3 days followed by incubation with 2 ug/ml CXCL12 for 2 days. Inhibition of CXCR4 induces significant inhibition of GSC chemotaxis in response to CXCL12 ($n = 12$ experiments for patient 1, $N = 5$ experiments for patient 2, $^{***}p < 0.001$, $^{*}p < 0.05$, Student's t-test).

an ex vivo 3D engineered biomimetic environment, we demonstrated that GliaTrap significantly attracts GSCs that are migrating away from patient-derived GSC tumor spheres. Finally, using X-CLARITY and 3D light-sheet microscopy, we confirmed that GliaTrap significantly attracts patient-derived GSCs in vivo using a human orthotopic xenograft glioblastoma model.

Cancer cell invasion away from the tumor bulk is one of the hallmarks of glioblastoma and significantly contributes to patient mortality. Here, we engineered GliaTrap to introduce a sustained chemoattractant gradient in the tumor microenvironment to revert the migratory stream of glioblastoma cells and confine them close to the tumor resection cavity.

Results

CXCL12 induces GSC chemotaxis via CXCR4

CXCL12 was previously shown to induce the chemotaxis of glioblastoma cells[15]. To confirm its functions as a chemoattractant for GSCs, we performed a chemotaxis assay in six patient-derived GSCs using Incucyte live-cell imaging. Our results show that treatment with CXCL12 induces a significant increase in the migration index of most GSCs (Fig. 1A).

CXCL12 has three known receptors: CXCR4, CXCR7, and ACKR1[16,17]. scRNA-seq data from the Brain Immune Atlas show that in glioblastoma the population of CXCR4 + cancer cells is about 60%, CXCR7 + cancer cells is about 2%, and ACKR1 + cancer cells are absent[18]. Thus, we hypothesized that CXCR4 is the major receptor responsible for CXCL12-induced chemotaxis. To test this hypothesis, first we examined the expression of CXCR4 in six patient-derived GSCs, which showed variable but universal CXCR4 expression (Fig. 1B). Then we inhibited the expression of CXCR4 with two individual siRNAs in GSCs and show that siCXCR4-2 is more potent in inhibiting CXCR4 expression (Fig. 1C) ($n = 3$, $^{*}p < 0.05$, $^{***}p < 0.0001$). Treatment of GSCs with siCXCR4-2 shows a significant decrease in the CXCL12 induced migration index of GSCs ($n = 2$ patients derived GSCs, $n = 12$ experiments for patient 1, $n = 5$ experiments for patient 2, $^{***}p < 0.001$, $^{*}p < 0.05$) (Fig. 1D). Finally, to exclude potential effects of CXCL12 on GSC proliferation, we treated 3 GSCs with 2 ug/ml CXCL12 and performed an MTS assay. This shows that the growth rate of CXCL12-treated GSCs was equal to that of non-treated GSCs, indicating that CXCL12 does not induce GSC proliferation (Fig. S1A).

Effects of CXCL12 on GSC transcript expression

To investigate the effect of CXCL12 on GSCs at the transcriptional level, we treated the GSCs with 2 ug/ml CXCL12 for two days and performed RNA-seq. Differential gene expression (DGE) analysis showed hundreds of differentially expressed genes, indicating that 2 ug/ml CXCL12 had a notable influence on transcripts in GSCs (Fig. S1B). To functionally classify the CXCL12 regulated transcripts, we performed gene set enrichment analysis (GSEA) on the DGE results and the functional pathways were ranked using GO. CXCL12-treated GSCs showed higher enrichment in chemotaxis signatures compared to non-treated GSCs, while the functional pathways pertaining to cell migration were ranked highest (Fig. S1C). To further investigate the effect of CXCL12 on transcriptional networks of GSCs, we performed weighted gene correlation network analysis (WGCNA). This analysis showed that CXCL12 transcripts correlate with CD248, SRGN, and ABI3BP genes, which are all responsible for cancer cell migration (Fig. S1D).

Generation of a biomimetic 3D device to study effects of CXCL12 on GSC migration

To generate a biomimetic 3D device that could harbor human glioblastoma spheroids and could be used to study migration of GSCs, we utilized collagen I as an extracellular matrix component and polydimethylsiloxane (PDMS). The device was designed such that the chemoattractant is released from the left side of the device to form a concentration gradient, which could be detected by the glioblastoma cells migrating out from the GSC spheroid implanted in the center of the device (Fig. 2A). To ensure that our biomimetic device can be used to test the effect of CXCL12 concentration gradient on the directional migration of GSCs, we tuned the overall dimensions of the device and the shape and size of the posts that delineate the CXCL12 chamber from the center chamber that harbors the GSC spheroid. The final device has the following overall dimensions: width 16 mm, height 8 mm, and depth 3.175 mm. The width of the left side (CXCL12) and center (GSC) chambers were 3.682 mm and 7.364 mm, respectively. We selected circular over rectangular or hexagonal posts for the posts separating the CXCL12 chamber from the GSC chamber since this post shape supported the best linear gradient

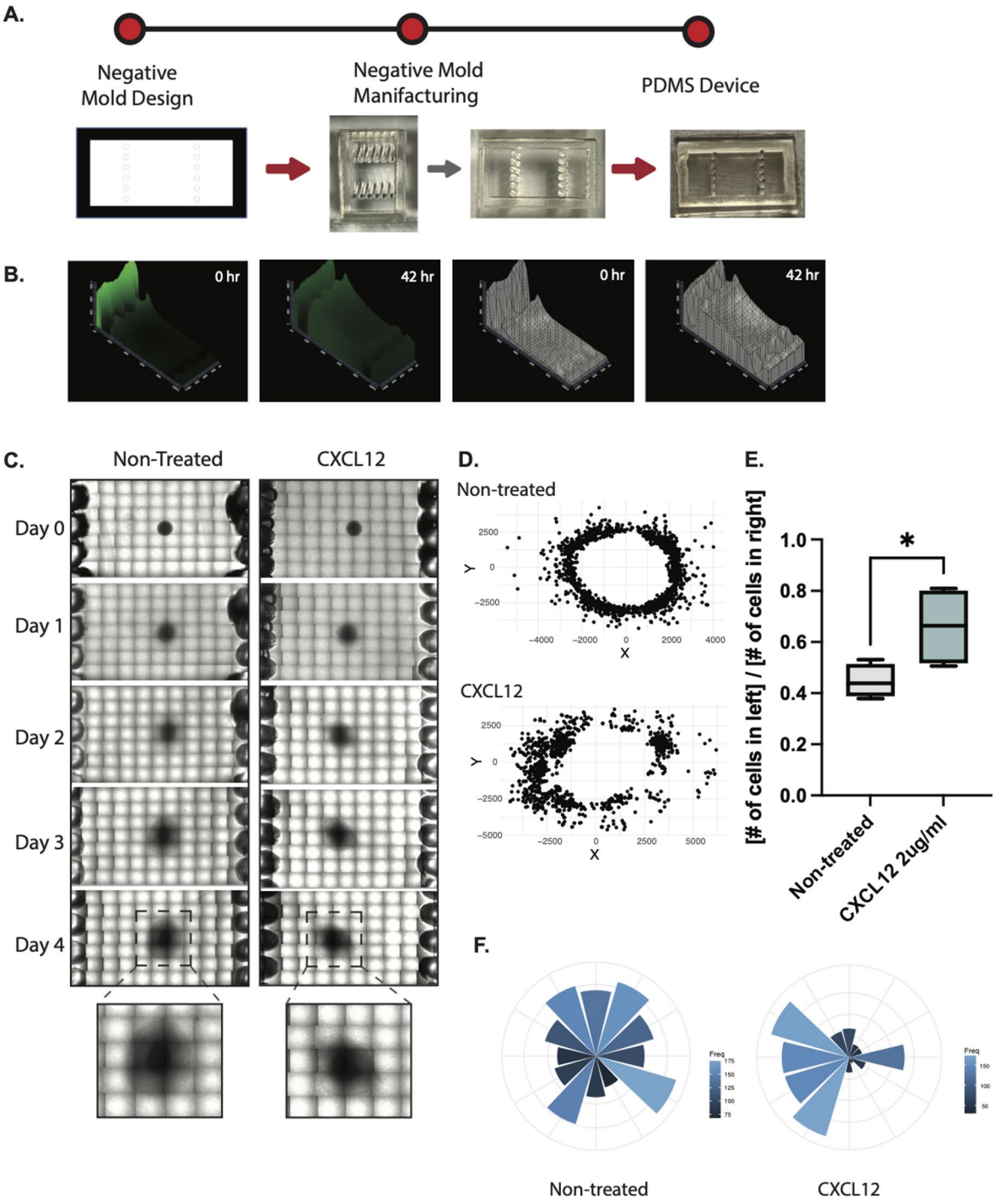

Fig. 2. CXCL12 induces GSC chemotaxis in a biomimetic device. (**A**) Design of the negative mold for the biomimetic device and development of the PDMS device. (**B**) Time-lapse images between T = 0 and T = 42 h for dextran release from our hyaluronic acid/collagen II-based (HA/Col) hydrogel in the device using Zen 2.5D visualization software (Zeiss). (**C**) Time-lapse images of GSC migration in the device in the presence or absence of GliaTrap + CXCL12. Images were acquired each day for 4 consecutive days. GSC spheroids were embedded in the middle chamber of the device in Collagen I. (**D**) Coordinates of each migrating GSC in control or GliaTrap devices at day 4 were plotted using R. (**E**) Quantification of the ratio of migrating GSCs between the left and right side of the middle line of each GSC spheroid. GliaTrap induces significant increase in the number of GSCs migrating towards the GliaTrap containing chamber of the device (*$p < 0.05$, Student's t-test). (**F**) Coordinate single cell migration data were used to calculate the polar coordinates and degrees from the origin and visualized as a rose plot using the R package ggplot2.

effect. Finally, we tested different numbers of posts and different distances between posts and determined that six posts with 0.653 mm distance between the posts provides the ideal environment for CXCL12 linear gradient formation. We used our optimized device with fluorescent dextran (10 kDa), which is a fluorescence molecule with a similar size to CXCL12, in the left chamber of the device and observed the release of dextran into the collagen I environment in the center chamber for 42 h (Fig. 2B). This showed a linear gradient formation and continuous release of dextran into the center chamber suggesting that this architecture of the device is suitable for studying the effects of CXCL12 on GSC migration.

CXCL12 concentration gradient attracts GSCs migrating from a glioblastoma spheroid

Using our biomimetic 3D device, we tested the effect of CXCL12 on GSCs migrating radially from a tumor spheroid. We transferred 2 ug/ml CXCL12 in the collagen I mixture in the left chamber of the device and a GSC tumor spheroid in the center chamber of the device and observed the GSC migration for four days using live cell microscopy (Fig. 2C). To quantify the effect of CXCL12 on GSC migration, we measured the number of GSCs that migrated towards the left and the right chambers after four days and calculated the ratio of cells towards the left versus the right. This shows that CXCL12 induces a significantly higher ratio of cells migrating towards the CXCL12 chamber (left) as compared to the negative control (non-treated) (Fig. 2D, E). Then we mapped the angles and coordinates of each individual cell migration in relation to the GSC tumor spheroid and quantified the effect of CXCL12 on the directionality of cellular migration. This quantification showed that CXCL12 induces a significant increase in directional migration towards the CXCL12 chamber (Fig. 2F) validating that a CXCL12 concentration gradient preferentially attracts GSCs migrating out from a glioblastoma tumor spheroid.

Characteristics of the HA/Col II hydrogel containing liposome encapsulated CXCL12

To maintain protein stability and achieve sustained release of CXCL12 from the hydrogel, we encapsulated CXCL12 in liposomes and formulated a CXCL12 liposome embedded hydrogel. CXCL12 loaded liposomes were 217.1 ± 20.45 nm in size with a particle size distribution (PDI) of 0.353 ± 0.022 nm and neutrally charged with a zeta potential around 0 mV. The CXCL12 loading efficiency was 99.8%. The liposomes were mixed with the hydrogel materials prior to the gelation process. As shown Fig. 3A, the liposome-HA/Col II hydrogel mixture was in a liquid state at room temperature and gelled quickly at 37 °C in approximately two minutes, through crosslinking between succinimidyl groups of PEG and amine groups of collagen II. The ratio of storage modulus to loss modulus of the liposome-HA/Col hydrogel composite was around 50, confirming that the mixture was gel-like status, not suspension. The storage modulus of the liposome-HA/Col hydrogel composite was 234.41 ± 9.09 Pa, which is comparable to that of many soft tissues including the brain (~ 140–620 Pa)[19], suggesting that the developed liposome/hydrogel composite may be well tolerated in the brain tissues. The swelling property of the HA/Col II hydrogel and liposome/hydrogel composite were also investigated. The swelling ratio of the HA/Col II hydrogel and liposome-HA/Col II hydrogel in the artificial cerebrospinal fluid at 37 °C was 5.18% ± 0.46% and 4.39% ± 0.69%, respectively showing no significant difference (Fig. 3B). This confirmed that our hydrogel system had low swelling in the aqueous environment. More importantly, the liposome-HA/Col II hydrogel demonstrated sustained release of CXCL12 over two weeks with a steady daily payload release (Fig. 3C).

CXCL12 liposome-embedded HA/Col II hydrogel has no inflammatory side effects in vivo

To verify the gelation of HA/Col hydrogel at body temperature (37 °C), we created an in vitro environment that mimics the stiffness and temperature of the mouse brain by pre-warming Matrigel to 37 °C (Fig. S2A). Afterward, we loaded fluorescent dextran (10 kDa) into a liquid HA/Col II mixture and injected the dextran-loaded mixture into the pre-warmed Matrigel using the same injection method as that in the in vivo experiment. We confirmed that dextran diffusion of the HA/Col II hydrogel group was much slower than that of the dextran in DPBS group (Fig. S2B), indicating that the HA/Col II hydrogel becomes a gel quickly at 37 °C (normal body temperature).

CXCL12 has been shown to exhibit both pro- and anti- inflammatory properties[20–22]. To examine whether the CXCL12 released from our hydrogel induces an inflammatory reaction in the brain, and to exclude the possibility that our hydrogel itself induces any inflammatory response, we performed stereotactic injections of the GliaTrap (CXCL12 liposome embedded HA/Col II hydrogel), blank liposome-embedded HA-Col II hydrogel, HA/Col II hydrogel only and DPBS as a control in the brain of C57/B6 immune competent mice. One week later, we harvested the mouse brains (Fig. S2C) and performed mouse cytokine array analysis on the brain lysates. The result showed that the GliaTrap, the blank liposome-embedded HA/Col II hydrogel and the HA/Col II hydrogel did not significantly affect cytokines compared with the DPBS control group (Fig. 3D, E). To visually quantify any effect of GliaTrap on inflammatory cell infiltration in the brain, we performed immunohistochemistry on coronal brain Sect. (4 µm thickness) at the level of injection site across three experimental groups using $N = 3$ mice per group: subhippocampal needle stick only, injection of hydrogel vehicle only, and injection of hydrogel containing CXCL12 (GliaTrap). We stained the slides with F4/80 to identify macrophages; CD4 to identify CD4 + T-Cells; CD8a to identify CD8 + T-Cells; and Granzyme B to identify activated T cells and natural killer cells. All antibodies and concentrations were quality tested using mouse spleen sections as positive control (Fig. S3). We detected F4/80 positive macrophages in all three groups adjacent to the injection site (purple arrows), but not in slices prepared using the other three antibodies (Fig. 4). GliaTrap visibly attracted macrophages to the hydrogel site compared to widespread macrophage infiltration observed in needle only or hydrogel only controls (Fig. 4, purple arrows).

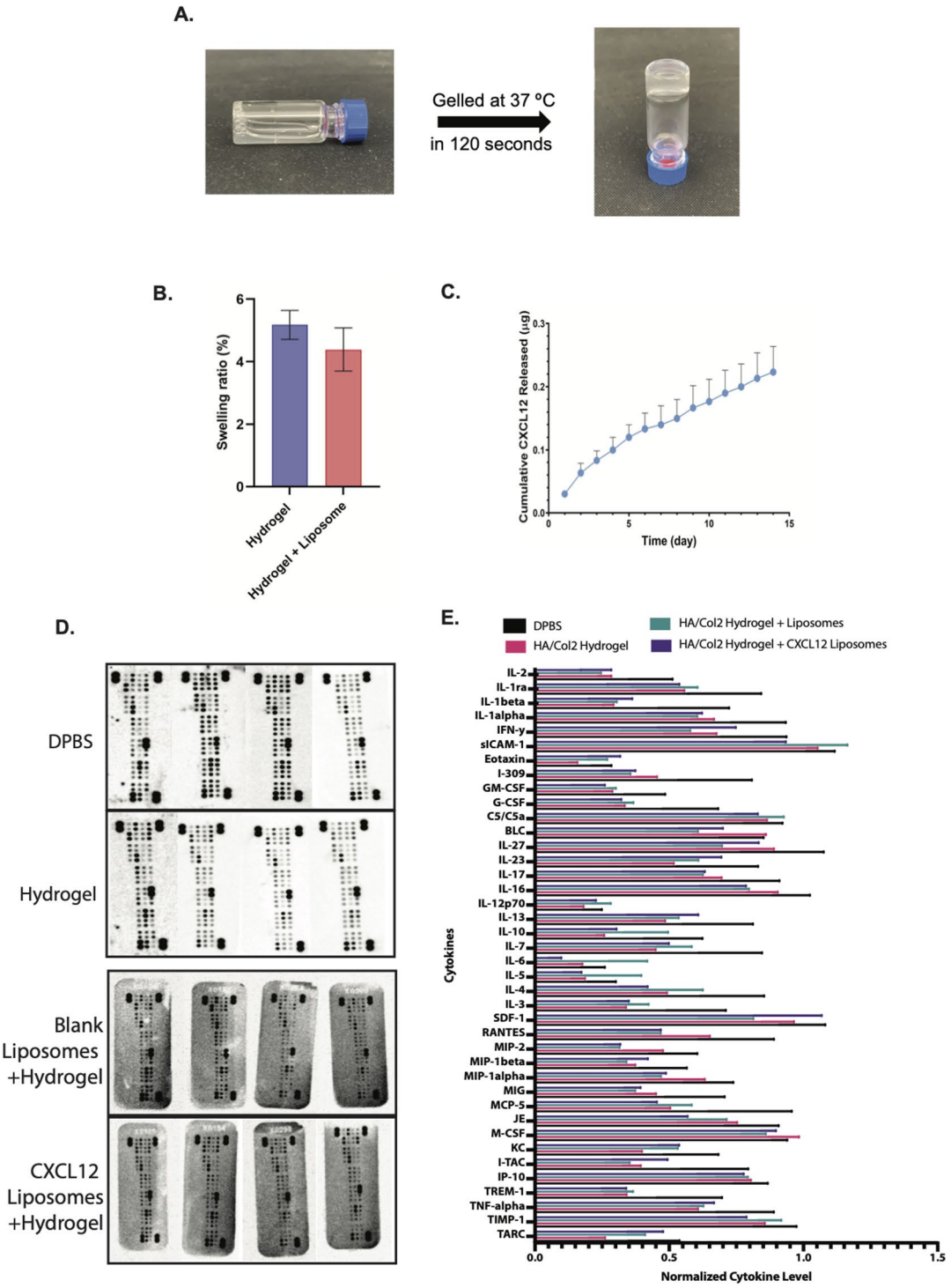

GliaTrap disperses along blood vessels in the brain

Since GliaTrap is thermoactivated, injected as a liquid, and becomes a gel at body temperature, we examined if injection of GliaTrap in the brain parenchyma could form gel projections along preexisting structures in the brain like blood vessels. We loaded fluorescent dextran as shown above and injected the dextran loaded GliaTrap in the brain of Balb/C mice ($n = 3$). One hour after the injection, mice were sacrificed and the brains were processed for tissue clearing using X-CLARITY, a lipid-targeting tissue-clearing technique which has been used to study cell movement in the mouse brain at a single-cell resolution due to its tissue-clearing quality and relatively fast runtime[23,24] (Fig. S2C). Following tissue clearing, the brains were stained for smooth muscle actin to label blood vessels and imaged with a 3D light sheet microscope (Olympus). This showed that GliaTrap forms several projections within the brain parenchyma following existing blood vessel formations (Fig. 5A, arrows) and even covers some blood vessels in the vicinity of the injections site (Fig. 5A, inset arrowheads).

◂**Fig. 3**. GliaTrap composed of hyaluronic acid/Col II hydrogel does not swell, provides sustained release of CXCL12, and does not cause inflammation in vivo. (**A**) The gelation time of GliaTrap was determined using a tube inversion method at 37 °C. (**B**) The swelling ratio of GliaTrap was studied in an artificial cerebrospinal fluid. GliaTrap shows low (up to 5%) swelling (the difference between hydrogel and hydrogel + liposome depicted at the bar graph is not significant). (**C**) In vitro CXCL12 release kinetics from GliaTrap show sustained release of CXCL12 over 15 consecutive days. The cumulative amount of CXCL12 was measured by ELISA. (**D**,**E**) Cytokine arrays using brain lysates from control mice (DPBS), mice with implanted HA/Col II hydrogel only, mice with implanted HA/Col II hydrogel + Blank liposomes and mice with implanted GliaTrap (HA/Col II hydrogel + CXCL12-loaded Liposomes). Quantification of the amount of each cytokine of each group was performed by calculating [signal intensity of a dot for each cytokine]/[signal intensity of reference dot] and comparison were performed with Anova. GliaTrap does not have any effect on pro-inflammatory cytokine levels in the brain.

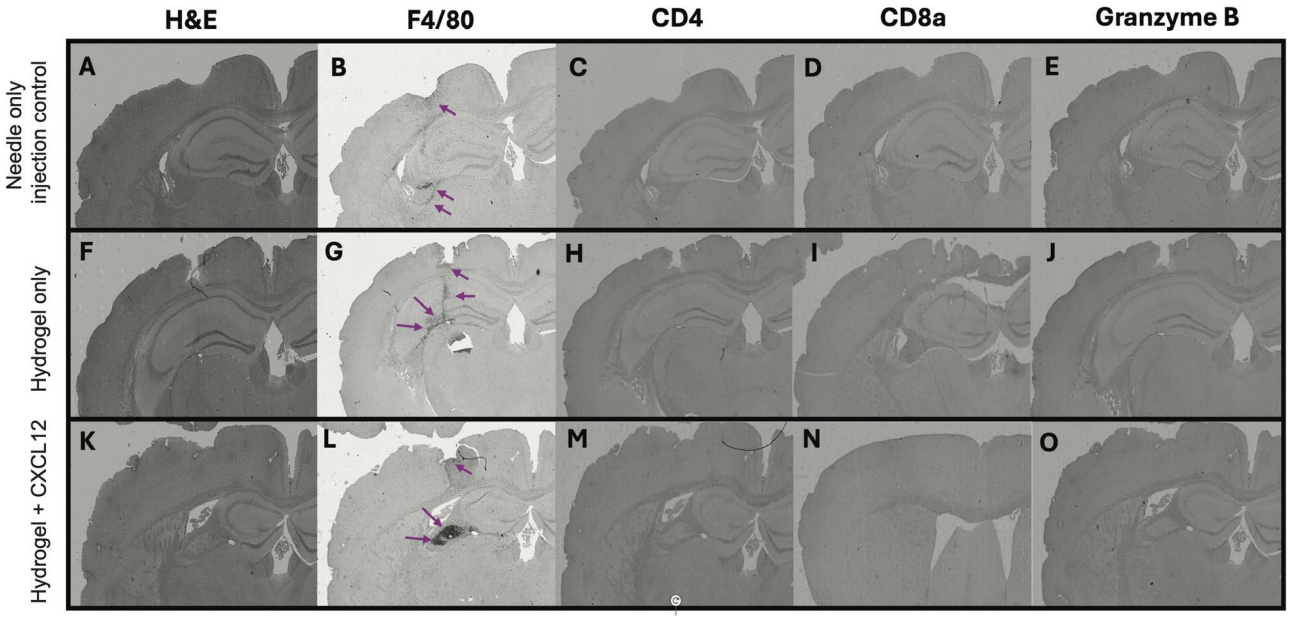

Fig. 4. GliaTrap does not induce inflammatory infiltration in vivo. Mouse brain coronal Sect. (4 μm thickness) at the level of injection site across three experimental groups: subhippocampal needle stick only (**A**–**E**), injection of hydrogel vehicle only (**F**–**J**), and injection of hydrogel containing CXCL12 (GliaTrap) (**K**–**O**). Representative images are shown, chosen from among $n = 3$ mice in each experimental group. From left to right, slices were prepared with H&E staining; F4/80 mAb 1:250 to identify macrophages; CD4 mAb 1:100 to identify CD4 + T-Cells; CD8a mAb 1:400 to identify CD8 + T-Cells; and Granzyme B mAb 1:100 to identify activated T cells and natural killer cells. All antibodies and concentrations were the same as for spleen positive control staining from the injection-only mice, as shown in (Supplementary Fig. 3). Antibody positivity was observed in F4/80 in all three groups adjacent to the injection site (purple arrows), but not in slices prepared using the other three antibodies. Images were captured using an Axio Observer Z1/7 microscope, Axiocam 705 1X Camera Adapter, and EC Plan-Neuofluar 10X / 0.30 M27 Objective.

GliaTrap attracts migrating GSCs from glioblastoma tumors in vivo

To investigate the efficacy of GliaTrap (CXCL12 liposome-embedded HA/Col II hydrogel) in vivo, we injected 500,000 ZsGreen-expressing human GSCs into eight Nu/J mice at coordinates of −2.0 mm AP and +1.5 mm ML relative to Bregma and −3.5 mm DV. These coordinates reflect the anatomic location of the putamen (subhippocampal region). The GSCs used for the in vivo experiment had high expression of CXCR4 and responded very significantly to CXCL12 induced migration (GSC3 cells from Fig. 1A, B). One week later, we implanted GliaTrap into the brains of $N = 4$ mice and empty liposome-embedded HA/Col II hydrogel into the other $N = 4$ mice at 1.0 mm above the tumor injection site and monitored these mice for an additional week. Injection coordinates were selected because anatomically they pinpoint the cortical region above the hippocampus, through which glioblastoma cells usually do not migrate[25]. We posited that if human GSCs migrate through the hippocampal region, it will provide stronger evidence for the power of GliaTrap to attract migrating cancer cells. During the one week of monitoring after the implantation of GliaTrap, no motor deficit nor other abnormal behavior was observed, indicating that the GliaTrap did not induce any symptomatic neurological damage either by hydrogel swelling or inflammatory reaction. A week after GliaTrap implantation, we harvested the brains and performed X-CLARITY. Following X-CLARITY, the processed brains were imaged using a 3D light-sheet microscope (Olympus). To measure the human GSCs migrating away from the tumor mass, we first defined the

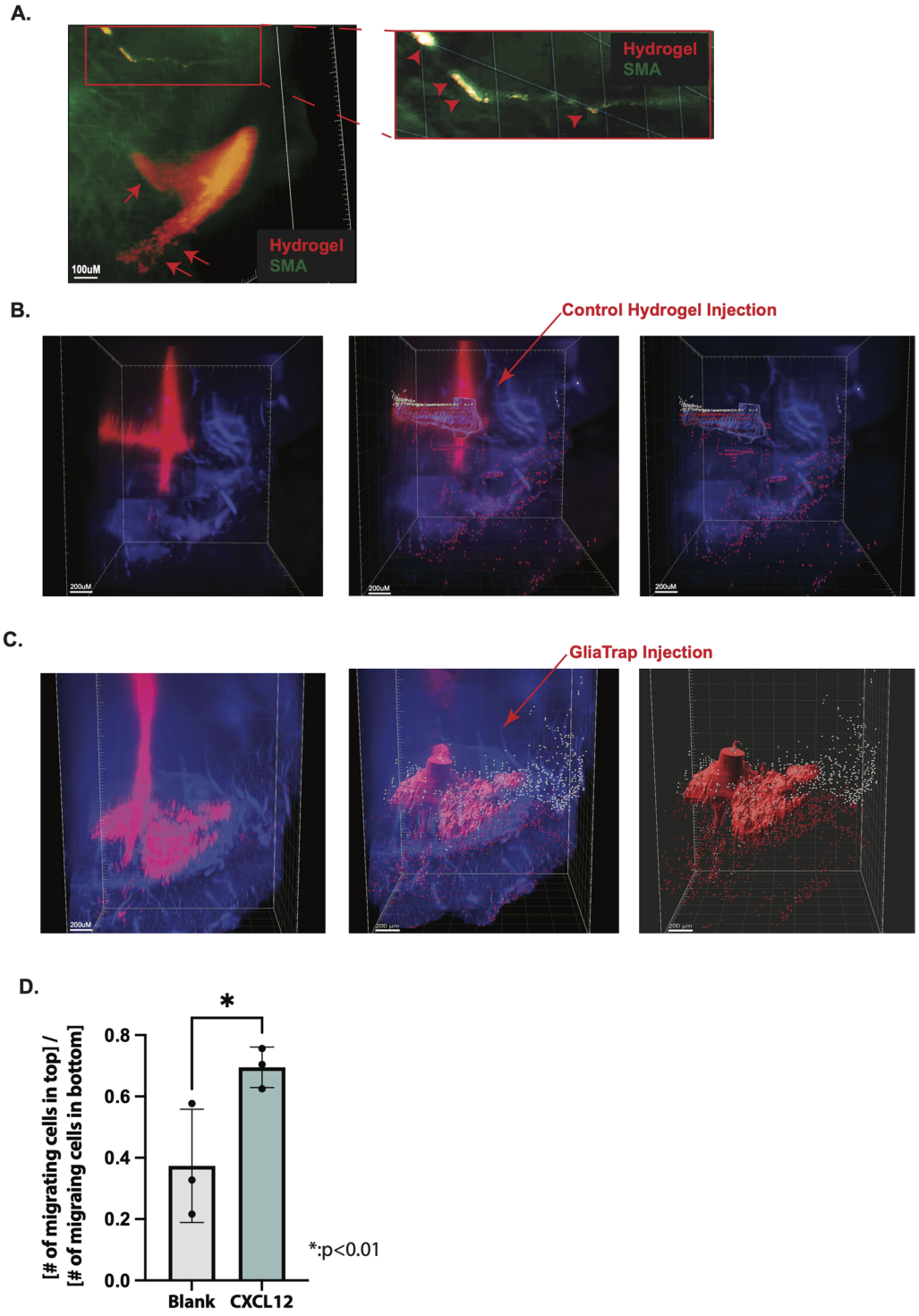

tumor mass area and the migrating GSCs based on the local maxima of signal intensity. To show preferential migration of human GSCs from the tumor mass towards GliaTrap, we measured the number of migrating GSCs above and below the tumor mass-defined region. We observed that GliaTrap induced a significant ($p < 0.01$) increase in the ratio of cells migrating at the area above the tumor where GliaTrap was implanted relative to the region below the tumor (Fig. 5B–D).

Discussion

In situ gelling hydrogels have attracted considerable interest in the past decade, owing to their advantages over pre-formed rigid polymeric implants such as Gliadel®. These advantages include: (1) excellent injectability with minimal required operative invasiveness; (2) the ability to conform to the available space or cavity of the injection site maximizing contact between the hydrogel and tissue, thereby enhancing payload access to tumor tissues; and (3) tunable mechanical properties that ensure compatibility with the surrounding brain tissues.

◀**Fig. 5**. GliaTrap disperses along blood vessels in the brain and attracts migrating GSCs in vivo. (**A**) Representative 3D-light sheet image of dextran-contained GliaTrap (pseudo-colored red) showing gel projections along pre-existing blood vessels stained with smooth muscle actin (arrows). Inset shows a magnified image of a brain blood vessel (green) covered with the GliaTrap hydrogel (arrows). (**B**) Representative 3D light sheet images of the control group of mice ($n=4$). Human glioblastoma tumor (red) and single glioblastoma cells migrating mainly below the tumor mass are shown. Arrow depicts the area where the control (blank) hydrogel was injected under stereotactic guidance. (**C**) In mice implanted with GliaTrap ($n=4$), single glioblastoma cells are migrating below (red) and above (white) the tumor mass. Arrow depicts the area where the GliaTrap was injected under stereotactic guidance. All images were processed using Imaris Imaging Software. (**D**) Quantification of the ratio of migrating cells above the center line of the tumor mass to those below the center line shows that GliaTrap induces significant increase in the number of migrating glioma cells towards the GliaTrap injection site above the tumor mass, confirming the chemoattracting properties ($n=6$, $^*p<0.01$, Student's t-test).

The HA/Col II hydrogel is mainly composed of natural biopolymers collagen and HA and hence possesses superior biocompatibility compared to synthetic biodegradable polymers such as poly(lactic-co-glycolic acid) which degrades into monomers that acidify the local environment leading to potential local inflammatory reaction[26]. It is noteworthy that our hydrogel system had low swelling in the aqueous environment which is ideal for maintaining good biocompatibility with surrounding tissues, particularly in the brain, as demonstrated in the present research using a patient-derived xenograft mouse model. In these models, hydrogels were injected directly into the tumor-invading center since resection of the tumor is not readily possible in this experimental system, but subsequent in-human or large animal safety evaluations could further confirm these properties if GliaTrap is deployed into a resection cavity.

Furthermore, our hydrogel comprised primarily of HA and Col II demonstrated low immunogenicity, with only minimal response of macrophages and no response of T-cells and natural killer cells at the site of injection and hydrogel implant. Only marginal increase in macrophage response was seen in the GliaTrap, and only confined to the cite of the implanted gel. Some localized innate immune response is expected following any injury to brain tissue, including intracerebral injection. It is possible that the GliaTrap further attracts these localized and highly motile macrophages into the gel itself, explaining why increased staining was observed in the GliaTrap mice at the site of the hydrogel implantation. These findings support the overall safety profile of GliaTrap as a potential delivery platform which should be further investigated for delivery of a variety of chemoattractant and tumor-killing molecules.

The characteristic finger-like invasion pattern of glioblastoma cells around existing brain structures (myelinated white matter, blood vessels, axonal tracks) was first described by Scherer[27] in the 1930s. CXCL12 is highly expressed in these structures and contributes to the induction of migration of CXCR4-positive glioblastoma cells[28–30]. The ability of CXCL12 to guide glioblastoma cell migration has been supported by in vitro experiments[13,31], however the molecular mechanisms involved are not completely defined[32,33]. The role of CXCL12 in modulating the activity of CXCR4 and CXCR7 in GSCs[34], as well as the function of CXCL12 as a mediator of GSC radiation resistance in the subventricular zone[35], have been documented. Though these studies confirm the potent pro-migratory and chemoattractant role of CXCL12 for GSCs, they also suggest a possible adverse pro-tumorigenic role. Accordingly, to safely employ CXCL12 as the chemoattractant for GliaTrap requires controlled release both in terms of concentration and duration. Alternative chemoattract agents could also be considered.

Here, we showed that GliaTrap can achieve tuned release of CXCL12 durable over weeks and that in vivo application of GliaTrap releasing CXCL12 in the brain induces minimal pro-inflammatory reactivity from the tumor microenvironment. To maximize the effectiveness of GliaTrap and to mimic Scherer structures in the brain by creating artificial finger-like projections of the hydrogel, we also designed GliaTrap to be thermo-reactive. GliaTrap is initially injected as liquid at room temperature so it can disperse in the interstitial space, where it polymerizes among longitudinally oriented tissue structures within the brain in reaction to the increased body temperature. Since the hydrogel projections of GliaTrap contain liposome-encapsulated CXCL12, allowing the gel to disperse freely before solidifying and therefore better recapitulating Scherer structures provides a more physiological environment to attract migrating glioma cells expressing CXCR4.

Our work proves that GliaTrap containing CXCL12 efficiently attracts a significant portion of migrating glioma cells in orthotopic in vivo models of human glioblastoma, however it does not address how these attracted glioma cells could be eliminated. In future applications, we could take advantage of the liposomes embedded within GliaTrap, to preload with therapeutic agents like antibodies, chemotherapeutics, RNA molecules, aptamers etc. This approach will help deliver therapeutic agents locally in the brain in the vicinity of glioblastoma cells and bypass the blood brain barrier. In conclusion, we envision GliaTrap as a delivery platform that could deliver various chemoattractant molecules and therapeutics into the brain and other solid tumors.

Materials and methods

Primary glioblastoma stem cell isolation and culture

Collection of human tumor tissue was approved by the Rhode Island Hospital IRB for the generation of cell lines used in our in vitro and in vivo experiments. All collections were performed with written informed consent from patients, samples were de-identified prior to use in research, and the studies were performed in accordance to recognized ethical guidelines (Belmont Report). Primary GSC spheres were cultured from human glioma samples as previously described[36]. GSCs used in this study were authenticated by ATCC using short

tandem repeat (STR) analysis. GSCs used were between passages 5 and 30 and cultured either as spheres or as attached on fibronectin-coated plates (10 ug/ml, Millipore Sigma) in a medium of 1X Neurobasal Medium, 2% B27 serum-free supplement, minus Vitamin A, 100X Glutamax (final concentration: 2mM) (Fisher Scientific), 1 mg/ml Heparin (STEMCELL Technologies), 20 ng/ml epidermal growth factor (Peprotech), 20 ng/ml basic-fibroblast growth factor (Peprotech). All GSC cultures are routinely tested for mycoplasma contamination using the MycoSensor qPCR assay (Agilent).

Lentiviral transduction of glioblastoma stem cells

Lentivirus containing pHAGE-EF1a-ZsGreen-IRES-puromycin plasmid was concentrated by ultracentrifugation at 99,800xg for 90 min, then virus pellets were suspended in HBSS (Gibco). The virus titer was determined with Lenti-X™ p24 Rapid Titration ELISA Kit (Takara), according to the manufacturer's instructions. GSCs (1×10^5/12 well) were transduced in condition media by spin-infection (940xg) at 32 °C for 2 h. Puro-resistant and ZsGreen-positive GSCs were generated after seven days of puromycin selection, and the purity of stable GSCs was confirmed by flow cytometry analysis.

In-vitro live-imaging chemotaxis assay

Inserts and reservoirs in an IncuCyte ClearView migration plate (Essen BioScience, 4582) were coated with a solution consisting of 10 ug/ml fibronectin (Sigma, FC0105MG) to 1% BSA (Fisher Scientific, NC0582624) in HBSS (Gibco, 14025076) at 37 °C for 30 min. GSCs were resuspended at a concentration of 66,666 cells/ml in NBA complete media. After aspiration from inserts and reservoirs, a 60ul cell suspension containing 4,000 cells was seeded into the inserts and allowed to rest at room temperature for 15 min. Complete media or complete media containing 2 ug/ml of CXCL12 (Fisher Scientific, 350-NS-050) (200 ul) was added to the appropriate reservoirs. The IncuCyte ClearView cell migration plate was placed into the IncuCyte instrument SX1 (Essen BioScience) and scanning with a 10x objective lens for every 2 h was scheduled over 120 h according to the manufacturer's instructions. Normalized migration indices were calculated by normalizing the area of cells in the reservoir at 48 h to the initial area of cells in the insert.

In-vitro proliferation assay

In-vitro proliferation assay was performed using MTS assay. GSC 4,000 cells were treated with CXCL12 2 ug/ml for five days in complete culture media (200 ul) in Nunc™ MicroWell™ 96-Well, Nunclon Delta-Treated, Flat-Bottom Microplate (ThermoFisher) pre-coated with fibronectin. Five days later, MTS reagent 20 ul (Abcam, ab197010) was added to each well, and the absorbance at 490 nm was measured every 30 min for 4 h at 37 °C. Absorbance at 490 nm was plotted using GraphPad Prism version 9.4.1. Cell morphology was observed every 2 h during the five days using IncuCyte® live-cell imaging.

SiRNA transfection

GSCs were grown in a fibronectin-coated plate and transfected with 50 nM siRNA targeting CXCR4 (Dharmacon, L-005139-00-0005) or a non-targeting control siRNA (Dharmacon, D-001810-10-05) by using Opti-MEM (Gibco, 31985062) and the TransIT-X2® Dynamic Delivery System (Mirus, 6000) in complete media without heparin (StemCell Tech, 07980) and Anti-Anti (Fisher Scientific, 15240062). The media was replaced with complete media without Anti-Anti 24 h after transfection. The cells were incubated for 48 more hours before they were lysed or used in subsequent experiments.

Western blot analysis

Cell lysates were prepared in 1x SDS lysis buffer containing 10 mM protease inhibitor cocktail (Millipore Sigma, P8340-1ML) and quantified using the Qubit Protein Assay Kit (Fisher Scientific, Q33211). Protein samples (20 ug) were used to perform electrophoresis in 1x Bolt™ MOPS SDS Running Buffer (Fisher Scientific, B0001) in Tris-buffered saline containing Tween-20 (TBST) (Fisher Scientific, 28360) in a Bolt 4–15% Bis-Tris Plus gel (Fisher Scientific, NW04120BOX) following the manufacturer's instructions. The antibodies were incubated with primary antibody anti-CXCR4 (1:1000 in 5% BSA) (Abcam, ab181020) or β-actin (1:10000 in 5% milk in TBST) (Sigma, A1978) according to the manufacturer's instructions. The membranes were then incubated with HRP-conjugated secondary antibodies (Cell Signaling Technology) at room temperature for 1 h. The protein signals were detected using the chemiluminescent kit Radiance Q (Azure Biosystems AC2101). The western blot images were quantified by FIJI software[37] and normalized to the corresponding β-actin control. Full uncropped images of the Western blots included in the paper are presented in Fig. S4.

RNA sequencing and analysis

The 5×10^6 attached GSCs were treated with recombinant CXCL12 2 ug/ml for two days. GSCs were lysed using the Trizol reagent (Invitrogen). RNA was isolated from this lysate using the RNeasy mini kit (Qiagen). Next-generation sequencing was performed on these RNAs. Sequence reads were aligned to the human hg38 genome assembly with hisat2 [38]. Read counts were summarized with FeatureCounts using the refseq annotations found in the refGene.txt file (http://hgdownload.cse.ucsc.edu/goldenPath/hg38/database/refGene.txt.gz)[38]. Protein-coding genes were selected, and differential gene expression analysis was performed on these protein-coding genes using DEBrowser, a R package to detect changes in gene expression[38]. Eseq2, a R package, was used to perform differential gene expression analysis[39]. Genes with fold change > 1.5 and p-value < 0.05 were considered for functional analysis.

Gene set enrichment analysis

Gene Set Enrichment Analysis (GSEA) was performed on the outcome of differential gene expression analysis using GSEA (Version 4.1.0)[40] to see if particular sets of genes are enriched, such as chemotaxis, metastasis, proliferation, DNA damage, mesenchymal glioblastoma, and proneural glioblastoma.

Weighted gene correlation network analysis (WGCNA)

Weighted Gene Correlation Network Analysis (WGCNA) was performed using the WGCNA R package (Version 1.70-3) to identify gene and module networks that have similar gene expression patterns with CXCL12. Particularly, WGCNA was performed on publicly available GSC data[41]. Genes from the modules with the highest correlation and p-value < 0.05 were picked to show the CXCL12-associated network. This network was visualized using Cytoscape (Version 3.8.2)[42].

PDMS device design

The PDMS device was designed and manufactured for testing the CXCL12 concentration gradient by using a previously established method. The device's dimensions are width of 16 mm, height of 8 mm, and depth of 3.175 mm. The device is designed with round edges and has six posts on each side with diameters of 0.635 mm, and the distance between posts is 0.653 mm.

Chemoattractant kinetics imaging assay

Dextran (Thermo Fisher Scientific, D7170) 2.5 ug with collagen I mixture (100 ul) was loaded into the left chamber of the PDMS device. 0.1% BSA-containing DBPS in Cultrex rat Collagen I solution (R&D Systems, 3440-005-01) 170 ul was loaded in the center chamber, and 100 ul was loaded to the right chamber of the device. The dextran-containing collagen I mixture was polymerized at 37 °C first to prevent the release of dextran into the center chamber. The collagen mixture was loaded into the center and right chambers and then polymerized at 37 °C. After the polymerization, the device was imaged using Zeiss Apotome 2 with 10x magnification and tile mode. This procedure was done every 3 h for three days. The release was visualized using Zeiss imaging software Zen's 2.5D visualization mode.

3D model

The PDMS device is placed in a non-treated 6-well plate (USA Scientific, CC7672-7506) along with DPBS-soaked Kimwipe to avoid evaporation. One day before this GSC sphere invasion experiment, 100,000 GSCs in 200 ul were plated in a 96-well untreated round bottom plate (Corning, 351177). The plate was centrifuged at 110 rpm for 10 min at room temperature and was incubated at 37 °C 6% CO_2 for 24 h to allow the formation of a GSC sphere.

CXCL12 (200 ug/ml, R&D Systems, 350-NS-050), dissolved in 0.1% BSA in DPBS, in Cultrex rat Collagen I was added to the left side of the device, and 0.1% BSA-containing DBPS in collagen I solution was added to the right side of the device. After collagen I polymerization at 37 °C for 1 h, a GSC sphere was placed in NaOH-stabilized Cultrex rat collagen I (R&D Systems, 3440-005-01). To prevent incomplete and premature gelation of the collagen, the 60 mm untreated 6-well plate, the Eppendorf tubes, and the pipette tips were pre-cooled. The plate was then imaged using the Zeiss Apotome 2 with 10x magnification and tile mode. This procedure was done every 24 h for five days.

The number of migrating cells on both left and right sides of the sphere was quantified by FIJI. The final coordinate data was used to calculate the polar coordinates and degrees from the origin and visualized as a rose plot using the R package ggplot2 (ver. 3.3.6).

Preparation and characteristics of HA/Col II hydrogel

CXCL12-loaded liposomes were formed by mixing Lipofectamine 2000 (Thermo Fisher) and carrier-free human CXCL12 protein (R&D systems) at 1:1 molar ratio and the mixture was incubated at room temperature for 2 h. The particle size, size distribution (polydispersity index, PDI), and surface charge of liposomes were characterized using Zetasizer Nano ZS90 (Malvern Instruments Ltd., Malvern, UK). The backscattering angel was 173° with a standard laser wavelength λ of 633 nm. The measurements were carried out in triplicate. The CXCL12 loading efficiency (LE) was determined using an ultra centrifugal filter (Amicon®-0.5, 30 kDa MWCO, MilliporeSigma, Burlington, MA) to remove the free protein. Human CXCL12 ELISA kit (R&D systems) was used according to the manufacturer's protocol to quantify total protein in the liposomes before centrifugation and free protein in the receiving tube after the centrifugation. CXCL12 loading efficiency (LE) was calculated using the following equation:

$$LE\ (\%) = \frac{CXCL12\ total\ amount\ in\ the\ liposomal\ sample\ -\ CXCL12\ amount\ in\ the\ receiving\ tube}{CXCL12\ total\ amount\ in\ the\ liposomal\ sample} \times\ 100\%$$

Lipofectamine 2000 was studied as blank liposomes. CXCL12-loaded liposomes were stored at 4 °C until further use.

To form HA/Col II hydrogel, 5 mg/ml of HA solution in PBS (10 mM, pH 7.4) was mixed with 5 mg/ml of collagen II solution in 200 mM phosphate buffer (pH 7.4) (3/1, collagen II/HA, v/v). Following this, 200 mg/ml of 8-arm PEG succinimidyl glutarate (8-arm PEG) solution in PBS (10 mM, pH 7.4) was added into the mixture (1/13.5, v/v) and a HA/Col II hydrogel was formed following incubation at 37 °C To form liposome/hydrogel composite (CXCL12-loaded or blank liposome-HA/Col II hydrogel), liposomes were accurately added into the phosphate buffer (200 mM, pH 7.4) to obtain the collagen II solution prior to mixing with other gel components (i.e., HA and PEG). The liposome/hydrogel composite was then formed when incubating the mixture at 37 °C.

Gelation time of the liposome-HA/Col II hydrogel was assessed using a tube inversion method. Rheological properties of liposome-HA/Col II hydrogel were determined using a TA Discovery HR-2 rheometer (TA Instruments, New Castle, DE). The gel component mixture (800 µl) was immediately loaded on a sample plate that was pre-equilibrated at 25 °C, and the cone shape geometry (40 mm, 2°) was lowered to a gap of 48 µm. Storage modulus of the liposome-HA/Col II hydrogel was determined via unconfined compression measurements with oscillation frequency ranging from 0.1 to 10 Hz at 5% strain at 37 °C.

To evaluate swelling behavior of the hydrogel, disc-shaped liposome-embedded HA/Col II hydrogel samples were formed in a 96-well plate in triplicate. The sample was transferred into an Eppendorf tube and weighed on a microscale (Mettler Toledo, Greifensee, Switzerland) to obtain the initial weight (W_i). The sample was incubated in an artificial cerebrospinal fluid (aCSF, Tocris Bioscience) at 37 °C to allow free swelling for 48 h. The sample was then removed and excess aCSF was gently removed. The fully swollen samples (W_s) were recorded. Hydrogel swelling was calculated based on mass change percentage (%) using the following equation:

$$Mass\ increase\ (\%) = \frac{Ws - Wi}{Wi} \times 100\%$$

To determine CXCL-12 release in vitro, CXCL12-loaded liposome-HA/Col II hydrogel samples were pre-formed and incubated in 200 µl of aCSF. The samples were placed in a shaking water bath at 37 °C with 45 rpm shaking speed. At predetermined time points, supernatants were collected and replenished with fresh aCSF. CXCL12 released amount was determined using a human CXCL12 ELISA kit (R&D systems) after breaking liposomes using 1% of Triton X-100. Cumulative CXCL-12 released amount was then calculated.

In-vitro hydrogel gelation test

Gelation of the hydrogel was tested in an in-vitro environment that mimics the anatomy of the mouse brain. Matrigel (Corning, 354234) in DPBS was mixed and added to a 24-well plate, and this plate was incubated for at least 30 min to ensure the gelation of the Matrigel. Dextran, Oregon Green™ 488; 10 kDa, Anionic (D7170, Thermo Fisher Scientific) 25 mg/ml (1 ul) was mixed with 4 ul of DPBS. The diluted dextran (0.5 ul) was mixed with 100 ul of hydrogel components. The dextran-contained hydrogel component (2 ul) was injected into the pre-warmed Matrigel at -1.0 mm depth DV using a stereotactic injector with a 30G needle and Hamilton syringe at 0.5 ul/min. Right after the completion of the injection, the plate was imaged using Zeiss Apotome 2 with EGFP and a bright field at 10x magnification. This procedure was done with a tile mode (with tile size 10,000 µm x 10,000 µm and the number of tiles 224) and imaged at different time points (e.g., 30, 60, and 180 min).

Cytokine array analysis

Proteome Profiler Mouse Cytokine Array kit (R&D) was used to detect the potential immune-inflammatory proteins using capture antibodies in an ELISA format, which are on a membrane with their predetermined locations. The brain lysate was prepared by homogenizing the right hemisphere of the mouse brain with the frontal lobe removed in 500 ul of pre-chilled DPBS with a protease inhibitor cocktail. Triton-X 100 (1%) was added to the homogenized cell lysate and stored at -80 °C overnight. The thawed lysate was centrifuged at 10,000 xg for 5 min. Cytokine array assay was then performed on the supernatant of the mouse brain lysate by following the manufacturer's instructions. The spots in the image of the array were quantified using an image software, FIJI, and the signal was normalized by the reference spots.

In-vivo glioblastoma stem cell injection

All animal experiments were approved by Rhode Island Hospital's Institutional Animal Care and Use Committee (IACUC) and conformed to the relevant regulatory standards and overseen by the institutional review board. Female and male NU/J homozygous mice (9 weeks old) were obtained from Jackson Laboratory (RRID: IMSR_JAX:002019) and used for the stereotactic injections. The animals were housed together until the day before the surgery and then housed individually. Animals receiving treatment were randomly assigned. ZsGreen expressing GSCs suspension 1×10^5/ul in HPBS was prepared and loaded into a Hamilton syringe with a 30G needle. The tip of the needle was inserted into a 3.5 mm depth at a speed of 1.00 mm per minute. The needle was pulled back to 3.0 mm depth, and GSC suspension (2.0 ul) was injected at 0.5 ul/minute and rested for 15 min. The needle was pulled back at 1.00 mm per minute, and the hole was closed by Bonewax (Ethicon) and Vetbond (3 M).

In-vivo hydrogel implant

The experimental group animals received 10 µl of CXCL12-containing liposome (CL)-embedded hydrogel, while the control group animals received 10 µl of blank liposome (BL)-embedded hydrogel. For the CL animals, 6.9 µl of 5 mg/ml CXCL12-contained liposomes embedded collagen solution and 2.41 µL of 5 mg/ml HA in PBS solution were combined into a clean, sterile, and pre-chilled 1.5 ml Eppendorf tube. Following gentle vortex, 0.69 µL of 200 mg/mL 8-arm PEG was added to the tube. The hydrogel components were mixed gently and immersed in ice and subsequently injected into the mouse brain of the B6 mouse at coordinates of – 2.0 mm AP and + 1.5 mm ML relative to Bregma. Particularly, the syringe needle was lowered to -3.5 mm DV at a rate of 0.5 mm per minute, pulled up to -2.0 mm DV, and then injected with the hydrogel at 0.66 ul per minute. For the BL mice, the same procedure was followed except that 6.9 µl of 5 mg/ml liposome-contained collagen was used.

Anesthesia and euthanasia

3–4% Isoflurane in oxygen using an induction chamber and maintenance during surgery for anesthesia.

Mice were euthanized with administration of CO2. We confirmed death of the animals by cutting the diaphragm after CO2 administration. Death was determined by the absence of heart beat and respiratory movements. These methods are consistent with the 2022 AVMA Panel on Euthanasia.

Tissue clearing

The freshly harvested brains were fixed in 4% PFA at 4 °C overnight. Brains were rinsed with pre-chilled PBS several times and transferred to pre-chilled PBS. Brains were cleared using X-CLARITYTM Hydrogel Solution Kit (Ledogos), according to the manufactured protocol, and stored in PBS at room temperature. The stock solution was prepared by mixing 2.5 g of X-CLARITY Polymerization Initiator (Cat# 13104, Logos Biosciences) in 10 ml 1X PBS to make a 25% (W/V) solution. Aliquots of 0.5 ml per brain were used and can be stored at -20 °C for up to 6 months. After thawing the aliquot at 4 °C or on ice, we diluted the solution 100 times in X-CLARITY Hydrogel Solution (Cat# 13103, Logos Biosciences). The brains were incubated in the hydrogel mixture at 4 °C for 24 h. The sample should be fully submerged in the hydrogel mixture.

Hydrogel polymerization for 3D light sheet

The polymerization system's settings were: Vacuum −90 kPa, Temperature 37 °C, Timer 3 h, and vessel type tube. The tube's cap should not be tight to allow gas exchange during the procedure. After the incubation, the tubes were shaken for 1 min to dissociate the hydrogel from the tube. The sample was then placed in a fresh tube and rinsed with 1X PBS multiple times to remove the excess hydrogel.

Electrophoretic tissue clearing

The electrophoretic chamber was filled with electrophoretic tissue clearing solution (Cat#.

C13001, Logos Biosciences) before placing the sample holder in the chamber. The following.

settings were used for 16 to 18 h to clear a whole brain: Current 1 A, Temperature 37 °C, and Pump speed 30 rpm. The samples were checked every 6 to 8 h for clearing results. After removing the sample from the chamber, it was rinsed with 1X PBS several times. The sample appeared opaque and white in PBS.

Light sheet microscope

The mouse brain was placed in 60% 2,2'-thiodiethanol solution overnight prior to imaging. The cleared brain was imaged using the LaVision Ultramicroscope II light-sheet microscope (Olympus). To image the entire brain, the image of the brain was acquired in a mosaic mode with 10% overlap and Z-stack mode with a light-sheet thickness of 4.05 µm at magnification 2x. This image was analyzed by using the imaging software Imaris (Oxford Instruments, Version 10). The tumor was defined based on the signals around the tumor injection site, particularly the tumor surface as contrast with the loss of signals in the surrounding area. The concentrated signals along the injection site were considered an artifact. The migrating cells were defined as dots with a local maximum outside the defined tumor and artifact. The migrating cells on top of the tumor were defined as the migrating cells above the middle of the tumor in the Z-axis, and the migrating cells on the bottom as those below that. For the mosaic 3D video, the images were taken with 10% overlap, and Imaris Stitcher was used to stitch 3D tile data and to create a video.

Visualization of hydrogel distribution in the brain

The HA/Col II hydrogel components was prepared using the same formulation as described above. Dextran (25 mg/ml, 1.1 µl) was added to the mixture to form the dextran-loaded hydrogel, followed by the addition of a 200 mg/ml 8-arm PEG solution in PBS (10 mM, pH 7.4) (1/13.5, v/v). The dextran-loaded hydrogel (2 µl) was then injected into the mouse brain using a stereotactic device, at a speed of 0.666 µl/minute to a depth of 2 mm. One hour after the injection, the mouse was sacrificed and the brain was harvested, fixed in 4% PFA overnight, and transferred to pre-chilled PBS within 24 h. The brain went through the tissue clearing, hydrogel polymerization, and electrophoretic tissue clearing steps. Subsequently, the cleared brain was washed with PBST and transferred to 1:300 Anti-Actin, α-Smooth Muscle - Cy3™ antibody (Millipore Sigma) in PBST for staining of the blood vessels. The sample was washed with distilled water to remove phosphate. The sample was incubated at X-CLARITY™ Mounting Solution for 1 h at room temperature, followed by a rinse with fresh X-CLARITY™ Mounting Solution and additional incubation for 1–2 h.

Tissue preparation, immunostaining, and microscopy of brain & spleen tissue

Mouse brain and spleen coronal Sect. (4 µm thickness) were prepared with H&E staining; F4/80 mAb (Cell Signaling Technologies, Rabbit mAb #70076) 1:250 to identify macrophages; CD4 mAb (Cell Signaling Technologies, Rabbit mAb #25229) 1:100 to identify CD4 + T-Cells; CD8a mAb (Cell Signaling Technologies, Rabbit mAb # 98941) 1:400 to identify CD8 + T-Cells; and Granzyme B mAb (Cell Signaling Technologies, Rabbit mAb # 44153) 1:100 to identify activated T cells and natural killer cells. Images were captured using an Axio Observer Z1 / 7 microscope, Axiocam 705 1X Camera Adapter, and EC Plan-Neuofluar 10X / 0.30 M27 Objective.

Data availability

The RNA-seq data discussed in this manuscript have been deposited in NCBI's Gene Expression Omnibus and are accessible through GEO Series Accession Number GSE219288.

Received: 23 December 2024; Accepted: 16 May 2025
Published online: 22 May 2025

References

1. Champeaux Depond, C. et al. Survival after newly-diagnosed high-grade glioma surgery: what can we learn from the French National healthcare database? *Brain Tumor Res. Treat.* **12**, 162–171. https://doi.org/10.14791/btrt.2024.0020 (2024).
2. Stupp, R. et al. Radiotherapy plus concomitant and adjuvant Temozolomide for glioblastoma. *N Engl. J. Med.* **352**, 987–996. https://doi.org/10.1056/NEJMoa043330 (2005).
3. Stupp, R. & Weber, D. C. The role of radio- and chemotherapy in glioblastoma. *Onkologie* **28**, 315–317. https://doi.org/10.1159/000085575 (2005).
4. Singh, S. K. et al. Identification of a cancer stem cell in human brain tumors. *Cancer Res.* **63**, 5821–5828 (2003).
5. Singh, S. K. et al. Identification of human brain tumour initiating cells. *Nature* **432**, 396–401. https://doi.org/10.1038/nature03128 (2004).
6. Lee, J. et al. Tumor stem cells derived from glioblastomas cultured in bFGF and EGF more closely mirror the phenotype and genotype of primary tumors than do serum-cultured cell lines. *Cancer Cell.* **9**, 391–403. https://doi.org/10.1016/j.ccr.2006.03.030 (2006).
7. Soni, P. et al. CD24 and Nanog expression in stem cells in glioblastoma: correlation with response to chemoradiation and overall survival. *Asian Pac. J. Cancer Prev.* **18**, 2215–2219. https://doi.org/10.22034/APJCP.2017.18.8.2215 (2017).
8. Collin, E. C. et al. An injectable vehicle for nucleus pulposus cell-based therapy. *Biomaterials* **32**, 2862–2870. https://doi.org/10.1016/j.biomaterials.2011.01.018 (2011).
9. Xie, L., Yue, W., Ibrahim, K. & Shen, J. A long-acting Curcumin nanoparticle/in situ hydrogel composite for the treatment of uveal melanoma. *Pharmaceutics* https://doi.org/10.3390/pharmaceutics13091335 (2021).
10. Wareham, L. K., Baratta, R. O., Buono, D., Schlumpf, B. J., Calkins, D. J. & E. & Collagen in the central nervous system: contributions to neurodegeneration and promise as a therapeutic target. *Mol. Neurodegener.* **19**, 11. https://doi.org/10.1186/s13024-024-00704-0 (2024).
11. Wang, T. W. & Spector, M. Development of hyaluronic acid-based scaffolds for brain tissue engineering. *Acta Biomater.* **5**, 2371–2384. https://doi.org/10.1016/j.actbio.2009.03.033 (2009).
12. Zou, Y. R., Kottmann, A. H., Kuroda, M., Taniuchi, I. & Littman, D. R. Function of the chemokine receptor CXCR4 in haematopoiesis and in cerebellar development. *Nature* **393**, 595–599. https://doi.org/10.1038/31269 (1998).
13. Rubin, J. B. et al. A small-molecule antagonist of CXCR4 inhibits intracranial growth of primary brain tumors. *Proc. Natl. Acad. Sci. U S A.* **100**, 13513–13518. https://doi.org/10.1073/pnas.2235846100 (2003).
14. Goffart, N. et al. Adult mouse subventricular zones stimulate glioblastoma stem cells specific invasion through CXCL12/CXCR4 signaling. *Neuro Oncol.* **17**, 81–94. https://doi.org/10.1093/neuonc/nou144 (2015).
15. Bajetto, A. et al. Expression of CXC chemokine receptors 1–5 and their ligands in human glioma tissues: role of CXCR4 and SDF1 in glioma cell proliferation and migration. *Neurochem Int.* **49**, 423–432. https://doi.org/10.1016/j.neuint.2006.03.003 (2006).
16. Gutjahr, J. C. et al. The dimeric form of CXCL12 binds to atypical chemokine receptor 1. *Sci. Signal.* **14** https://doi.org/10.1126/scisignal.abc9012 (2021).
17. Shi, Y., Riese, D. J., Shen, J. & 2nd & The role of the CXCL12/CXCR4/CXCR7 chemokine Axis in Cancer. *Front. Pharmacol.* **11**, 574667. https://doi.org/10.3389/fphar.2020.574667 (2020).
18. Pombo Antunes, A. R. et al. Single-cell profiling of myeloid cells in glioblastoma across species and disease stage reveals macrophage competition and specialization. *Nat. Neurosci.* **24**, 595–610. https://doi.org/10.1038/s41593-020-00789-y (2021).
19. Rowland, M. J. et al. An adherent tissue-inspired hydrogel delivery vehicle utilised in primary human glioma models. *Biomaterials* **179**, 199–208. https://doi.org/10.1016/j.biomaterials.2018.05.054 (2018).
20. Dotan, I. et al. CXCL12 is a constitutive and inflammatory chemokine in the intestinal immune system. *Inflamm. Bowel Dis.* **16**, 583–592. https://doi.org/10.1002/ibd.21106 (2010).
21. Garcia-Cuesta, E. M. et al. The role of the CXCL12/CXCR4/ACKR3 axis in autoimmune diseases. *Front. Endocrinol. (Lausanne).* **10**, 585. https://doi.org/10.3389/fendo.2019.00585 (2019).
22. McCandless, E. E., Wang, Q., Woerner, B. M., Harper, J. M. & Klein, R. S. CXCL12 limits inflammation by localizing mononuclear infiltrates to the perivascular space during experimental autoimmune encephalomyelitis. *J. Immunol.* **177**, 8053–8064. https://doi.org/10.4049/jimmunol.177.11.8053 (2006).
23. Lee, E. et al. ACT-PRESTO: rapid and consistent tissue clearing and labeling method for 3-dimensional (3D) imaging. *Sci. Rep.* **6**, 18631. https://doi.org/10.1038/srep18631 (2016).
24. Chung, K. et al. Structural and molecular interrogation of intact biological systems. *Nature* **497**, 332–337. https://doi.org/10.1038/nature12107 (2013).
25. Mughal, A. A. et al. Patterns of invasive growth in malignant gliomas-the hippocampus emerges as an invasion-spared brain region. *Neoplasia* **20**, 643–656. https://doi.org/10.1016/j.neo.2018.04.001 (2018).
26. Bruggeman, J. P., de Bruin, B. J., Bettinger, C. J. & Langer, R. Biodegradable poly(polyol sebacate) polymers. *Biomaterials* **29**, 4726–4735. https://doi.org/10.1016/j.biomaterials.2008.08.037 (2008).
27. Scherer, H. J. A critical review: the pathology of cerebral gliomas. *J. Neurol. Psychiatry.* **3**, 147–177. https://doi.org/10.1136/jnnp.3.2.147 (1940).
28. Ehtesham, M., Winston, J. A., Kabos, P. & Thompson, R. C. CXCR4 expression mediates glioma cell invasiveness. *Oncogene* **25**, 2801–2806. https://doi.org/10.1038/sj.onc.1209302 (2006).
29. Zagzag, D. et al. Hypoxia- and vascular endothelial growth factor-induced stromal cell-derived factor-1alpha/CXCR4 expression in glioblastomas: one plausible explanation of Scherer's structures. *Am. J. Pathol.* **173**, 545–560. https://doi.org/10.2353/ajpath.2008.071197 (2008).
30. Munson, J. M., Bellamkonda, R. V. & Swartz, M. A. Interstitial flow in a 3D microenvironment increases glioma invasion by a CXCR4-dependent mechanism. *Cancer Res.* **73**, 1536–1546. https://doi.org/10.1158/0008-5472.CAN-12-2838 (2013).
31. Bajetto, A. et al. CXCR4 and SDF1 expression in human meningiomas: a proliferative role in tumoral meningothelial cells in vitro. *Neuro Oncol.* **9**, 3–11. https://doi.org/10.1215/15228517-2006-023 (2007).
32. Woerner, B. M., Warrington, N. M., Kung, A. L., Perry, A. & Rubin, J. B. Widespread CXCR4 activation in Astrocytomas revealed by phospho-CXCR4-specific antibodies. *Cancer Res.* **65**, 11392–11399. https://doi.org/10.1158/0008-5472.CAN-05-0847 (2005).
33. Sciaccaluga, M. et al. Functional cross talk between CXCR4 and PDGFR on glioblastoma cells is essential for migration. *PLoS One.* **8**, e73426. https://doi.org/10.1371/journal.pone.0073426 (2013).
34. Wurth, R., Bajetto, A., Harrison, J. K., Barbieri, F. & Florio, T. CXCL12 modulation of CXCR4 and CXCR7 activity in human glioblastoma stem-like cells and regulation of the tumor microenvironment. *Front. Cell. Neurosci.* **8**, 144. https://doi.org/10.3389/fncel.2014.00144 (2014).
35. Goffart, N. et al. CXCL12 mediates glioblastoma resistance to radiotherapy in the subventricular zone. *Neuro Oncol.* **19**, 66–77. https://doi.org/10.1093/neuonc/now136 (2017).
36. Zepecki, J. P. et al. Regulation of human glioma cell migration, tumor growth, and stemness gene expression using a Lck targeted inhibitor. *Oncogene* https://doi.org/10.1038/s41388-018-0546-z (2018).
37. Schneider, C. A., Rasband, W. S. & Eliceiri, K. W. NIH image to imageJ: 25 years of image analysis. *Nat. Methods.* **9**, 671–675. https://doi.org/10.1038/nmeth.2089 (2012).
38. Kim, D., Paggi, J. M., Park, C., Bennett, C. & Salzberg, S. L. Graph-based genome alignment and genotyping with HISAT2 and HISAT-genotype. *Nat. Biotechnol.* **37**, 907–915. https://doi.org/10.1038/s41587-019-0201-4 (2019).

39. Love, M. I., Huber, W. & Anders, S. Moderated Estimation of fold change and dispersion for RNA-seq data with DESeq2. *Genome Biol.* **15**, 550. https://doi.org/10.1186/s13059-014-0550-8 (2014).
40. Subramanian, A. et al. Gene set enrichment analysis: a knowledge-based approach for interpreting genome-wide expression profiles. *Proc. Natl. Acad. Sci. U S A.* **102**, 15545–15550. https://doi.org/10.1073/pnas.0506580102 (2005).
41. Langfelder, P. & Horvath, S. WGCNA: an R package for weighted correlation network analysis. *BMC Bioinform.* **9**, 559. https://doi.org/10.1186/1471-2105-9-559 (2008).
42. Gustavsen, J. A., Pai, S., Isserlin, R., Demchak, B. & Pico, A. R. RCy3: network biology using cytoscape from within R. *F1000Res* **8**, 1774. https://doi.org/10.12688/f1000research.20887.3 (2019).

Acknowledgements

We would also like to thank Drs. Margot Martinez Moreno and Emily Arner for performing proof-of-concept experiments during the initial conceptualization phase of this project. We would like to thank Rajeev Kant and Amanda Khoo for their help in designing the PDMS device. We would like to thank the Neurobiology Imaging Facility at Harvard Medical School for consultation and instrument availability that supported this work. This facility is supported in part by the Neural Imaging Center as part of an NINDS P30 Core Center grant #NS072030. We thank the Lentivirus Construct Core of the Center for Stem Cells and Aging at Brown University supported by a COBRE grant from the National Institutes of Health (P20 GM119943).

Author contributions

Conceptualization: NT, Methodology: NT, JS, YS, Investigation: YS, DM-T, SM, MP, OL, WY, LX, BA, NP, EF, AF, Visualization: YS, NT, Funding acquisition: NT, JS, Supervision: NT, JS, Writing—original draft: YS, NT, Writing—review & editing: NT.

Funding

Funding for this work was provided by a Warren Alpert Foundation Grant to NT and the recruitment package from Brown University and Rhode Island Hospital for NT.

Declarations

Competing interests

The authors declare no competing interests.

Statements

All animal work included in this study, is reported according to ARRIVE guidelines. Collection of deidentified human tumor tissue was approved by the Rhode Island Hospital IRB (#405616).

Additional information

Supplementary Information The online version contains supplementary material available at https://doi.org/10.1038/s41598-025-02977-x.

Correspondence and requests for materials should be addressed to N.T.

Reprints and permissions information is available at www.nature.com/reprints.

Publisher's note Springer Nature remains neutral with regard to jurisdictional claims in published maps and institutional affiliations.